Evolution of the Kondo resonance feature and its relationship to spin-orbit coupling across the quantum critical point in $Ce_2Rh_{1-x}Co_xSi_3$

Swapnil Patil, V. R. R. Medicherla, R. S. Singh, E. V. Sampathkumaran, and Kalobaran Maiti*
Department of Condensed Matter Physics and Materials Science,
Tata Institute of Fundamental Research, Homi Bhabha Road, Colaba, Mumbai 400 005, India
(Dated: October 14, 2011)

We investigate the evolution of the electronic structure of $Ce_2Rh_{1-x}Co_xSi_3$ as a function of x employing high resolution photoemission spectroscopy. Co substitution at the Rh sites in antiferromagnetic Ce_2RhSi_3 leads to a transition from an antiferromagnetic system to a Kondo system, Ce_2CoSi_3 via the Quantum Critical Point (QCP). High resolution photoemission spectra reveal distinct signature of the Kondo resonance feature (KRF) and its spin orbit split component (SOC) in the whole composition range indicating finite Kondo temperature scale at the quantum critical point. We observe that the intensity ratio of the Kondo resonance feature and its spin orbit split component, KRF/SOC gradually increases with the decrease in temperature in the strong hybridization limit. The scenario gets reversed if the Kondo temperature becomes lower than the magnetic ordering temperature. While finite Kondo temperature within the magnetically ordered phase indicates applicability of the spin density wave picture at the approach to QCP, the dominant temperature dependence of the spin-orbit coupled feature suggests importance of spin-orbit interactions in this regime.

PACS numbers: 71.27.+a, 71.28.+d, 75.30.Fv

I. INTRODUCTION

Quantum criticality[1] in heavy fermion systems is obtained by tuning the antiferromagnetic phase transition temperature to zero by external non-thermal control parameter like pressure, chemical composition, magnetic field *etc.* The study of quantum criticality has attracted a great deal of attention recently due to the finding of non Fermi liquid excitations in the properties of metals near the magnetic instability in correlated systems and in particular in unconventional superconductors. The quantum critical point (QCP) separates two entirely different ground states - (i) long range magnetically ordered state and (ii) paramagnetic/nonmagnetic Fermi liquid state.[2] While the physics in the ground states on either sides, away from the QCP are reasonably well understood, the physics in the vicinity of QCP is a long standing puzzle.[3–5] The question to be answered is, how the quantum critical fluctuations affects the electronic excitations and how it evolves as one goes from one side of QCP to the other side.

In order to address the issue, we studied an archetypical systems $Ce_2Rh_{1-x}Co_xSi_3$ - the compounds in the whole composition range crystallize in a AlB_2 derived hexagonal structure with space group $P6/mmm$ as shown in Fig. 1.[6–8] The valence band consists of Si $3p$, Co $3d$ and Rh $4d$ electronic states.[9,10] Since the binding energy of the $4d$ electronic states is higher than the $3d$ electronic states and $3d$ electrons are relatively more correlated due to smaller radial extension,[11,12] the substitution of Co at Rh sites influences the effective d-p hybridization as well as the itineracy of the conduction electrons that leads to a plethora of interesting properties. For example, one of the end members, Ce_2RhSi_3 exhibit antiferromagnetic ordering at about 7 K.[6] Various

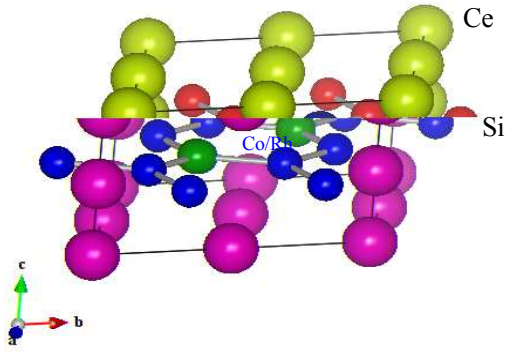

FIG. 1: Crystal structure of $Ce_2Rh_{1-x}Rh_xSi_3$ forming in AlB_2 type hexagonal structure.

studies involving lattice compression/expansion via external pressure or chemical substitutions suggested that this compound lies close to the peak of Doniachs magnetic phase diagram.[13,14] The sample with $x = 0.6$ composition exhibits quantum critical behavior such as non-Fermi liquid behavior in the electrical transport measurements. The compositions with $0.0 < x < 0.6$ exhibit antiferromagnetic ordering. It was shown that application of high pressure on the compounds in this composition range leads to a change in properties similar to that observed via change in composition.[15] The magnetic susceptibility measurements on the other end member, Ce_2CoSi_3, does not show magnetic ordering down to 0.5 K akin to a Kondo lattice compound with an estimated Kondo temperature, T_K of about 44 K. The temperature dependence of electrical resistivity of Co-end members

appear to be similar to a typical mixed valent Kondo lattice system.[6,16]

In this article, we present our results of investigation on the evolution of electronic structure as a function of Rh/Co concentration employing high resolution photoemission spectroscopy. The high resolution spectra exhibit distinct signatures of Kondo resonance feature and its spin orbit coupled component in the whole composition range. The relative intensity of the Kondo resonance feature with respect to the spin orbit split feature exhibits distinctly different temperature evolution in the different parts of the phase diagram.

II. EXPERIMENTAL DETAILS

High quality samples of $Ce_2Rh_{1-x}Co_xSi_3$ for various values of x were prepared in the polycrystalline form by arc melting - growth of the material from congruently molten phase ensured large grain size with homogenous stoichiometry. The samples are characterized by x-ray diffraction, transport and magnetic measurements as described elsewhere.[6] The photoemission measurements were carried out using high resolution Gammadata Scienta electron analyzer, SES2002 and monochromatic photon sources at a base pressure better than 3 $\times$ 10^{-11} torr. The energy resolutions were set to 300 meV at Al $K\alpha$ (1486.6 eV) photon energy, and 5 meV at He II (40.8 eV) and He I (21.2 eV) photon energies. The samples were very hard and could not be cleaved or fractured. Hence, the sample surface was cleaned by *in situ* scraping at each temperature using a fine grained diamond file and the surface cleanliness was ensured by the absence of O 1s and C 1s signals. The reproducibility of the spectra was ensured after each trial of surface cleaning. The Fermi level was determined at each temperature by measuring the Fermi cutoff in the spectral function of high purity silver mounted in electrical contact with the sample. The temperature variation down to 5 K was achieved using a open cycle helium cryostat, LT-3M from Advanced Research Systems, USA.

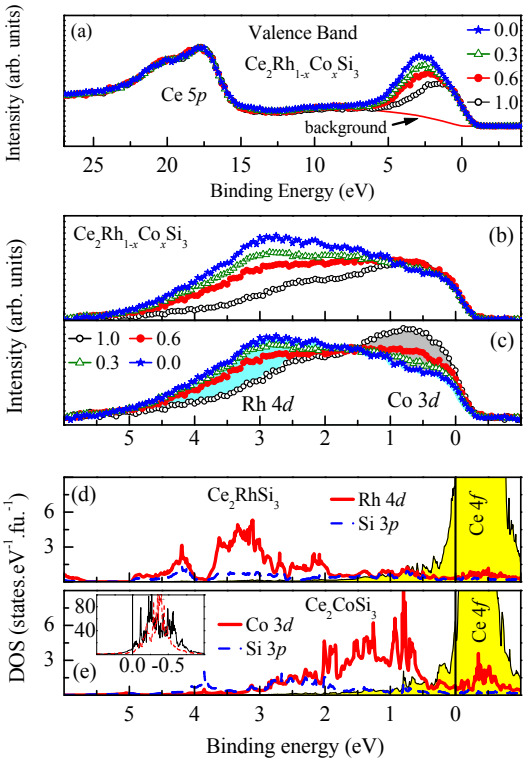

FIG. 2: (a) XP valence band spectra of $Ce_2Rh_{1-x}Co_xSi_3$ for various values of x at 5 K. The solid line shows a typical integral background function. (b) Background subtracted high resolution valence band spectra exhibiting evolution of the spectra with x at 5 K. (c) The same background subtracted spectra shown after normalization at 1.5 eV binding energy to demonstrate how the spectral intensity changes with composition. The gray shade shows the increase in Co 3d intensity and blue shade shows subsequent decrease in Rh 4d intensities with the increase in x. LDA results of the partial density of states of (d) Ce_2RhSi_3 and (e) Ce_2CoSi_3. The y-scale is expanded to visualize the Ce 4f (yellow shaded region), Si p and Co/Rh d partial density of states (PDOS) in the occupied part with clarity. The inset in (e) shows the Ce 4f PDOS for Ce_2CoSi_3 (dashed line) and Ce_2RhSi_3 (solid line).

III. RESULTS AND DISCUSSIONS

The photoemission measurements were carried out on four compositions, namely, x = 0.0 (antiferromagnetic), 0.3 (30% Co substituted and antiferromagnetic), 0.6 (corresponds to QCP), 1.0 (Kondo compound) that spans the whole range of the solid solution with varied properties. In Fig. 2(a), we show x-ray photoemission (XP; $h\nu$ = 1486.6 eV) valence band spectra collected at 5 K for the above four compositions (energy resolution used for these spectra = 0.6 eV). The spectra primarily consist of two groups of features. The signals corresponding to Ce $5p_{3/2}$ and $5p_{1/2}$ photoemission appear at 17.5 eV and 20.3 eV binding energies, respectively. The features close to the Fermi energy, ϵ_F constitute the valence band. Since Ce concentration is same in all the samples, the spectra have been normalized by the Ce 5p peak intensity. It is evident that the spectral weight around 2.8 eV gradually reduces with the decrease in Rh content.

To probe this region with greater clarity, we have obtained the high resolution (resolution = 0.3 eV) XP spectra of the valence band region close to ϵ_F as shown in Fig. 2(b) after integral background subtraction - a typical background function is shown in Fig. 2(a) by solid line. The spectral intensity within 1 eV of ϵ_F does not change significantly with x - a small increase is observed around 0.5 eV while there is a large decrease in intensity around 2.8 eV with the increase in Co content. Such an anomalous change can be attributed to the large photoemission cross-section of Rh 4d states ($\sim$ 0.012) compared

that for Co 3d states ($\sim$ 0.0037).[18] In order to visualize the spectral evolution due to substitution better, we renormalized the same spectra by the intensity at 1.5 eV binding energy as shown in Fig. 2(c). The increase in intensity corresponding to Co 3d photoemission is shown by gray shade and the decrease Rh 4d intensity is shown by blue shade - the gradual change in spectral intensities with the increase in x is beautifully manifested in the figure. These results suggest dominant Co 3d contributions close to ϵ_F, whereas Rh 4d contribute at higher binding energies.

The energy band structure calculations were performed for the end members Ce_2RhSi_3 and Ce_2CoSi_3 using full potential linearized augmented plane wave method (FLAPW) within the local density approximations using Wien2k software.[17] The lattice constants and all other structural details were obtained from the literature.[6] The calculated Ce 5p, Rh 4d/Co 3d and Si 3p partial density of states (PDOS) for Ce_2RhSi_3 and Ce_2CoSi_3 are shown in Fig. 2(d) and Fig. 2(e), respectively. The results reveal dominance of the contributions of Rh/Co d states in the valence band. The Rh 4d PDOS appear around 3 eV binding energies consistent with the experimental observations. The Co 3d states peak around 1 eV binding energy. Clearly, the calculated results correspond well with the experimental spectra shown in Fig. 2(c).

The d PDOS seem to have influenced the conduction electron-Ce 4f hybridization (cf-hybridization) significantly - Ce 4f PDOS width is broader in Ce_2RhSi_3 relative to that in Ce_2CoSi_3 as shown in the inset of Fig. 2(e). Moreover, the intensity of Co 3d PDOS in the Ce 4f region is stronger than the Rh 4d contributions in the same energy range. These observations suggest stronger Co 3d-Ce 4f hybridization than Rh 4d-Ce 4f hybridization. Evidently, proximity of the d states have strong influence on cf-hybridization[22] in addition to the influence of lattice volume change often referred in these systems.[6]

In Fig. 3, we compare the photoemission spectra collected using He Iα, He IIα and Al $K\alpha$ photon energies at 5 K. All the spectra are normalized by the intensities between 1 - 2.5 eV binding energy range. The features in He II and XP spectra are quite similar except the fact that the XP spectra are broader due to higher resolution broadening. Two distinct and sharp features appear in the vicinity of ϵ_F in the He II spectra of both Ce_2RhSi_3 and Ce_2CoSi_3.[9,10] The He I spectra, however, do not exhibit these intensities. Considering contributions of various electronic states near ϵ_F depicted in Figs. 2(d) and 2(e), and the dependence of their photoemission cross section,[18] the sharp features near the Fermi level can be attributed primarily to the photoemission from Ce 4f electronic states. The feature near ϵ_F corresponds to $4f_{5/2}$ photoemission and is a manifestation of the Kondo resonance features. The corresponding spin-orbit split component, the $4f_{7/2}$ final state appears at a relatively higher binding energies ($\sim$ 260 meV). In Fig. 3(c), we show the He II spectra of all the compositions at 5 K. Although the Rh 4d intensity gradually decreases with

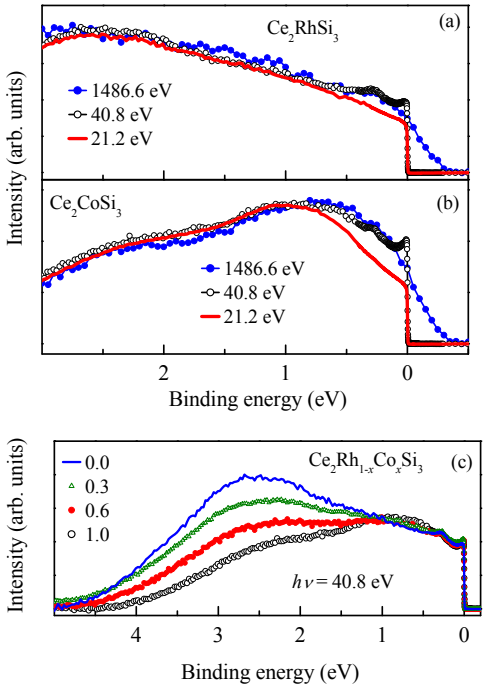

FIG. 3: Valence band spectra of (a) Ce_2RhSi_3 and (b) Ce_2CoSi_3 at 5 K obtained using different photon energies exhibiting results consistent with the band structure results. (c) He II spectra of $Ce_2Rh_{1-x}Co_xSi_3$ at 5 K for various values of x. The high energy resolution employed in this technique reveal distinct Kondo features near the Fermi level.

the increase in x as also observed in the XP spectra, the features near ϵ_F seems similar in the whole composition range.

Considering significant enhancement of the Ce 4f contributions in the He II spectra relative to the other contributions in the same energy region, one can extract the Ce 4f spectral function by subtracting the He I spectra from the He II spectra as often done in similar Ce-based systems. The peak of the Kondo resonance feature usually appears just above the Fermi energy (unoccupied) and the photoemission spectroscopy probes the higher binding energy tail of the Kondo peak.[19,20] Thus, the extracted 4f spectral weight by the difference (He II - He I) depicting the occupied part of the Ce 4f PDOS would provide a good estimation of the Kondo resonance feature.

The (He II - He I) spectra at different temperatures are shown in Fig. 4(a) for different compositions separately. The spectra of all the compositions exhibit a sharp feature near ϵ_F - the intensity of the feature reduces gradually with the increase in temperature suggesting presence of Kondo compensation effect in every case despite the fact that the magnetism in these materials are widely varied. The intensity of the Kondo resonance feature at a particular temperature gradually increases with the in-

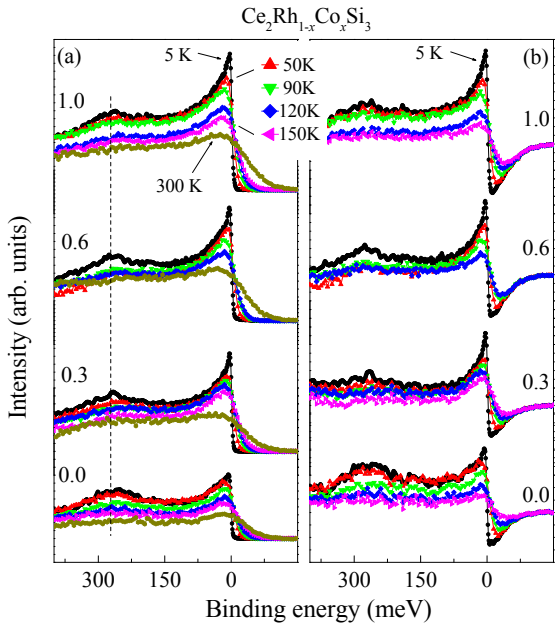

FIG. 4: (a) The evolution of the extracted Ce $4f$ spectral functions with temperature for different compositions. (b) The spectral weight transfer obtained by subtracting the room temperature spectra from the spectra at different temperatures.

crease in x. Since the Kondo temperature increases with the increase in x, the above observation suggests that the intensity of the Kondo resonance feature is directly related to the Kondo temperature, T_K.[5] While such a scenario is expected in a Kondo system, the similar observation in long range ordered systems ($x < 0.6$) indicates the existence of a finite Kondo temperature scale even in these cases.

The Kondo coherence temperature for the intermediate compositions estimated[6] from the electrical transport properties is ~ 8 K for $x = 0.3$ and ~ 50 K for $x = 0.6$. When the measurement temperature is below the coherence temperature, there will be additional complications due to the expansion of the Fermi volume and presumably manifested in the evolution of the Kondo resonance feature. The Kondo temperatures for the compositions, $x = 0.0$, 0.3 and 0.6 are 12 K, 30 K and 40 K, respectively.[6] The photoemission spectra collected at 120 K and 150 K are well above the coherence temperature, Kondo temperature and Néel temperature for all the compositions and still exhibit finite intensity of the Kondo resonance feature. At all the temperatures, we find qualitatively similar trend of the evolution of the Kondo resonance feature across the solid solution indicating that the spectral weight redistributions, if any, due to the onset of the Kondo coherence are not altering the inferences drawn. This manifests applicability of the single impurity Kondo physics in the electronic structure[23] and the Kondo temperature scale remains finite at the QCP.

The intensity of the corresponding spin-orbit split feature ($4f_{7/2}$ signal) appearing around 260 meV binding energy (marked by a vertical dashed line in Fig. 4(a)) in each of the samples also reduces as the temperature is increased. Interestingly, the intensity of the $4f_{7/2}$ signal seems to be similar in all the compositions although the intensity of the Kondo resonance feature at the Fermi level increases with the increase in Co concentration. At finite temperature, the spectral intensity representing the occupied part of the density of states becomes lower at ϵ_F due to the thermal effect represented by the Fermi-Dirac distribution function. The Fermi-Dirac distribution function depletes the intensity below ϵ_F and enhances the intensity above ϵ_F in a symmetric manner with the increase in temperature. We have subtracted the room temperature spectra from the spectra at different temperatures ($I(\epsilon, T) - I(\epsilon, 300K)$) to investigate the spectral weight transfer with temperature. Such exercise would provide a change in spectral weight symmetric with respect to the Fermi level in a Fermi liquid system. The subtracted spectral functions, shown in Fig. 4(b), however, exhibit asymmetric spectral evolutions with temperature - the gain of spectral weight below the Fermi level is larger than the loss of weight above the Fermi level. Such an effect appear in the presence of a peak such as Kondo resonance peak in the vicinity of the Fermi level. The asymmetry seems to be weaker towards Rh end indicating weaker Kondo peak. This clearly indicates that the temperature dependence of the Kondo peak and the spin-orbit peak is different.

To investigate the spectral changes with composition, x at a particular temperature, we re-plot the Ce $4f$ spectral functions as a function of composition at a particular temperature in Fig. 5(a). The experimental spectra exhibit gradual increase in intensity of both the peaks with the increase in x that can be associated to the change in the Kondo temperature as discussed above and also observed earlier in other Ce-based compounds.[5]

We compare the evolution of the intensities of the Kondo resonance peak and its spin-orbit split component in Fig. 6. In order to deconvolve the Fermi Dirac distribution induced depletion of the spectral density of states at the Fermi level, we symmetrized the spectra with respect to the Fermi level - if $I(\epsilon)$ represents the spectral function, the symmetrized spectra can be expressed as $I(\epsilon) = I(\epsilon - \epsilon_F) + I(\epsilon_F - \epsilon)$. It is often found that the intensity at the Fermi level can be estimated quite accurately by such symmetrization process, which is independent of the presence/absence of particle-hole symmetry. The symmetrized spectra are shown in Fig. 5(b) those represent the intensity of the Kondo resonance feature (KRF).

The estimated intensities of the spin orbit peak (SOC) obtained from Fig. 4(a) and the Kondo peak (KRF) obtained from Fig. 5(b) are shown in Fig. 6(a) (for Ce_2RhSi_3), 6(b) (for $Ce_2Rh_{0.7}Co_{0.3}Si_3$, 6(c) (for

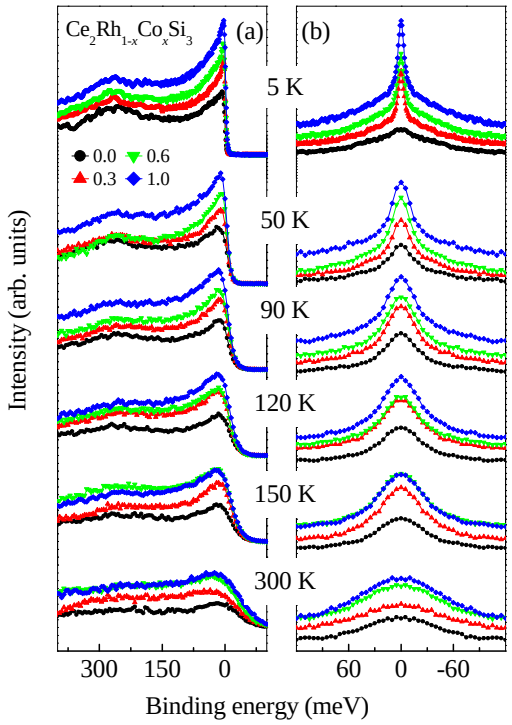

FIG. 5: (a) The evolution of the extracted Ce $4f$ spectral functions with composition, x at different temperatures. (b) The spectral functions obtained by symmetrizing the experimental spectra to estimate the spectral weight the Fermi level.

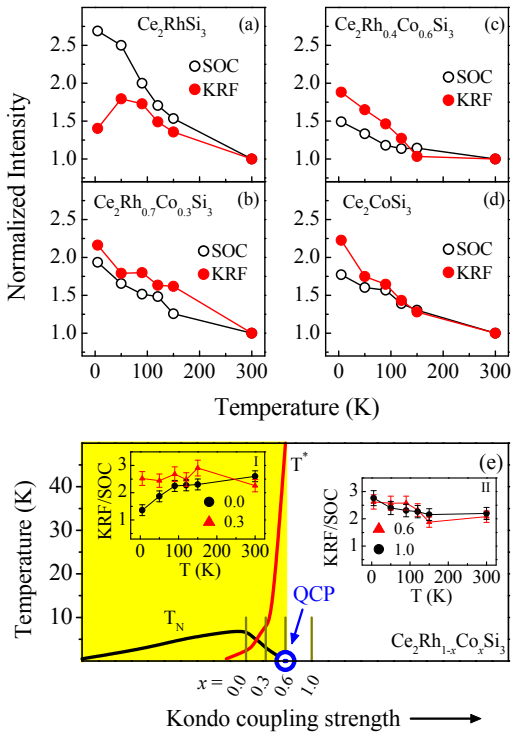

FIG. 6: Intensity variation of the Kondo resonance feature (KRF) and its spin orbit coupled (SOC) component as a function of temperature of (a) Ce_2RhSi_3, (b) $Ce_2Rh_{0.7}Co_{0.3}Si_3$, (c) $Ce_2Rh_{0.4}Co_{0.6}Si_3$ and (d) Ce_2CoSi_3. (e) A schematic phase diagram showing the long range ordered region (yellow) and Kondo compensated region separated by a quantum critical point (QCP). The left and right insets show the intensity ratio of KRF/SOC as a function of temperature for corresponding compositions in $Ce_2Rh_{1-x}Co_xSi_3$. T_N and T^* represent the Neél temperature and Kondo coherence temperature and are obtained from Ref. [6].

$Ce_2Rh_{0.4}Co_{0.6}Si_3$ and 6(d) (for Ce_2CoSi_3). Interestingly, the compositions exhibiting long range order show weaker temperature dependence of the Kondo resonance feature (KRF) compared to the spin orbit coupled (SOC) peak - the trend gets reversed on the other side of the phase diagram. This is shown by plotting the relative intensity ratio (KRF/SOC) in the insets of Fig. 6(e) in the corresponding phase regime. In the weak hybridization limit, the intensity ratio, KRF/SOC decreases with the decrease in temperature - the Kondo peak grows less rapidly than the spin orbit peak. On the other side (strong coupling limit), the ratio, KRF/SOC gradually increases with the decrease in temperature. Interestingly, the trend at the quantum critical point follows the strong coupling behavior.

Kondo effect essentially arises from the hybridization of the conduction electrons with the impurity moment. It is well known that in the strong coupling limit, the electrons corresponding to the local moment forms a quantum mechanically entangled states with the conduction electrons, termed as Kondo singlet. In such a scenario, the Fermi surface expands due to the additional contribution from the electrons forming the local moment - here the $4f$ electrons. The Kondo temperature essentially provides an energy scale deriving the expansion of the Fermi volume.[24,25] In many cases, it is observed that the Kondo temperature scale vanishes at the approach to QCP.[23,26] The results in the present study reveal finite Kondo temperature scale at the QCP in the solid solution $Ce_2Rh_{1-x}Co_xSi_3$ suggesting that the magnetic Ce $4f$ electrons near QCP acquire itineracy at lower temperatures - the antiferromagnetism near the QCP occurs among the itinerant electrons and hence indicates the applicability of an SDW picture in these cases.[9,15] Interestingly, the results in Fig. 6(e) suggests that if the Kondo temperature is higher than Néel temperature, the intensity of the Kondo resonance feature exhibits stronger temperature dependence compared to its spin-orbit split counterpart. The scenario gets reversed, if the Kondo temperature is lower than the ordering temperature.

IV. CONCLUSIONS

In summary, we studied the evolution of the electronic structure of $Ce_2Rh_{1-x}Co_xSi_3$ using high resolution photoemission spectroscopy. The signature of Kondo resonance feature is revealed in the high resolution low temperature spectra of all the compounds providing evidence of finite Kondo temperature scale at the quantum critical point. Interestingly, the temperature dependence of Kondo resonance feature is found to be stronger than its spin-orbit split counterpart if the Kondo temperature is higher than the magnetic ordering temperature. The spin-orbit part show stronger temperature dependence if the Kondo temperature becomes lower than the ordering temperature. While finite Kondo temperature scale in this regime establishes applicability of the spin density wave picture at the approach to the quantum criticality, the spin-orbit coupling appears to play a significant role in this regime. These results provide an insight to the origin of quantum fluctuations often observed in the proximity of the onset of exotic phases like superconductivity.

V. ACKNOWLEDGEMENTS

One of the authors S.P., thanks the Council of Scientific and Industrial Research, Government of India for financial support.

* Corresponding author: kbmaiti@tifr.res.in

[1] J. A. Hertz, Phys. Rev. B **14**, 7183 (1976).
[2] S. Doniach, Physica B & C **91**, 231 (1977).
[3] Q. Si, S. Rabello, K. Ingersent, and J. L. Smith, Nature **413**, 804 (2001).
[4] A. J. Millis, Phys. Rev. B **48**, 7183 (1993).
[5] M. Garnier, K. Breuer, D. Purdie, M. Hengsberger, Y. Baer, and B. Delley, Phys. Rev. Lett. **78**, 4127 (1997).
[6] S. Patil, Kartik K. Iyer, K. Maiti, and E. V. Sampathkumaran, Phys. Rev. B **77**, 094443 (2008).
[7] R. A. Gordon, C. J. Warren, M. G. Alexander, F. J. DiSalvo, and R. Pöttgen, J. Alloys Compds. **248**, 24 (1997).
[8] S. Majumdar, M. M. Kumar, R. Mallik, and E. V. Sampathkumaran, Solid State Comm. **110**, 509 (1999).
[9] S. Patil, V. R. R. Medicherla, R. S. Singh, S. K. Pandey, E. V. Sampathkumaran, and K. Maiti, Phys. Rev. B **82**, 104428 (2010).
[10] S. Patil, S. K. Pandey, V. R. R. Medicherla, R. S. Singh, R. Bindu, E. V. Sampathkumaran and K. Maiti, J. Phys.: Condens. Matter **22**, 255602 (2010).
[11] K. Maiti, U. Manju, S. Ray, P. Mahadevan, I.H. Inoue, C. Carbone, and D.D. Sarma, Phys. Rev. B **73**, 052508 (2006); K. Maiti, A. Kumar, D.D. Sarma, E. Weschke, and G. Kaindl, Phys. Rev. B **70**, 195112 (2004); K. Maiti and D. D. Sarma, Phys. Rev. B **61**, 2525 (2000).
[12] K. Maiti and R.S. Singh, Phys. Rev. B **71** 161102(R) (2005); K. Maiti, R.S. Singh, and V.R.R. Medicherla, Phys. Rev. B **76**, 165128 (2007); R. S. Singh, V. R. R. Medicherla, and K. Maiti, Appl. Phys. Lett. **91**, 132503 (2007).
[13] T. Nakano, K. Sengupta, S. Rayaprol, M. Hedo, Y. Uwatoko, and E. V. Sampathkumaran, J. Phys.: Condens. Matter **19**, 326205 (2007).
[14] I. Das and E. V. Sampathkumaran, J. Magn. Magn. Mater. **137**, L239 (1994).
[15] K. Mukherjee, K. K. Iyer, S. Patil, K. Maiti, and E.V. Sampathkumaran, J. Phys. Conf. Series **273**, 012010 (2011); K. Maiti, S. Patil, G. Adhikary, and G. Balakrishnan, J. Phys. Conf. Series **273**, 012402 (2011); K. Maiti, S. Patil, and E. V. Sampathkumaran, AIP Conf. Proc. **1347**, 181 (2011)
[16] J. M. Lawrence, P. S. Riseborough, and R. D. Parks, Rep. Prog. Phys., **44** 1 (1981).
[17] P. Blaha, K. Schwarz, G.K.H. Madsen, D. Kvasnicka, and J. Luitz, **WIEN2k**, An Augmented Plane Wave + Local Orbitals Program for Calculating Crystal Properties (Karlheinz Schwarz, Techn. Universität Wien, Austria), 2001. ISBN 3-9501031-1-2.
[18] J.J. Yeh and I. Lindau, At. Data Nucl. Data Tables **32**, 1 (1985).
[19] F. Patthey, W. -D. Schneider, Y. Baer, and B. Delley, Phys. Rev. Lett. **58**, 2810 (1987); F. Patthey, J. M. Imer, W. -D. Schneider, H. Beck, Y. Baer, and B. Delley, Phys. Rev. B **42**, 8864 (1990).
[20] D. Ehm, S. Hüfner, F. Reinert, J. Kroha, P. Wölfle, O. Stockert, C. Geibel, and H. v.Löhneysen, Phys. Rev. B **76**, 045117 (2007); M. Klein, A. Nuber, F. Reinert, J. Kroha, O. Stockert, and H. v.Löhneysen, Phys. Rev. Lett. **101**, 266404 (2008).
[21] O. Gunnarsson and K. Schönhammer, Phys. Rev. B **28**, 4315 (1983).
[22] O. Gunnarsson, N. E. Christensen, and O. K. Andersen, J. Magn. Magn. Mater. **76-77**, 30 (1988); doi:10.1016/0304-8853(88)90309-5.
[23] M. Klein, A. Nuber, F. Reinert, J. Kroha, O. Stockert, and H. v. Löhneysen, Phys. Rev. Lett. **101**, 266404 (2008).
[24] S.-I. Fujimori, Y. Saitoh, T. Okane, A. Fujimori, H. Yamagami, Y. Haga, E. Yamamoto, and Y. Onuki, Nat. Phys. (London) **3**, 618 (2007).
[25] P. Gegenwart, Q. Si, and F. Steglich, Nat. Phys. (London), **4**, 186 (2008).
[26] P. Gegenwart, T. Westerkamp, C. Krellner, Y. Tokiwa, S. Paschen, C. Geibel, F. Steglich, E. Abrahams, and Q. Si, Science, **315**, 969 (2007).